Percolation in nanocomposites with complex geometries: Experimental and Monte Carlo simulation studies

D. R. Stevens, L. N. Downen, and L. I. Clarke*
Department of Physics, North Carolina State University, Raleigh, North Carolina 27695, USA
(Received 18 August 2008; revised manuscript received 22 October 2008; published 19 December 2008)

The development of nanocomposites (a matrix, often polymeric, enhanced by a particle with a nanometer-sized dimension) has expanded dramatically in recent years with a particular focus on materials with complex microstructure and nanostructure. Such composites rely on formation of a connected network of particles throughout the sample volume in order to enhance the polymer's mechanical and electrical properties. From a fundamental perspective, this network formation will be governed by a percolation process within the constrained geometry of the particular microstructure. In this paper, the percolation process within a particular complex nanostructure, namely, a mat of electrospun nanofibers with fiber size of ≈ 100 nm and high porosity, is studied via continuum Monte Carlo simulations, where the sample geometry (fiber and particle sizes, orientation, and sample porosity) is matched to the mats utilized in our previous experimental work. A good agreement between experimental and computational results is observed. Simulations of spherical dopant in uniform samples, with zero, one, or two sample dimensions similar in size to the particle, were completed to explore the effects of confinement, in particular within a single fiber. These results were compared and contrasted with those from porous fibrous mats to determine the influence of porosity on the critical volume fraction. The results indicate that percolation in fibrous mats occurs via pathways that include sections of many fibers rather than being contained within single fibers which span the sample. The detailed dependence of critical volume fraction on porosity and the sensitivity to fiber number and width is discussed.

DOI: 10.1103/PhysRevB.78.235425 PACS number(s): 72.20.−i, 64.60.ah, 72.60.+g, 72.80.Tm

I. INTRODUCTION

Nanocomposite materials combine the high level processability of a polymer matrix with an enhancement of its mechanical, electrical, or chemical properties (e.g., drug delivery or catalysis) by addition of minute amounts of a particle with a nanometer-sized dimension (e.g., metal nanoparticles or carbon nanotubes).[1–4] For example, introduction of less than 1% volume fraction of multiwalled carbon nanotubes (MWNTs) increases a composite's electrical conductivity by more than 10 orders of magnitude.[5,6] Conductivity is imparted to the matrix when sufficient doping occurs such that networks of particle are formed, providing conducting paths that span the sample. Network formation is a percolation phenomenon, which depends on sample geometry and particle size and shape. The relatively facile processing of polymer materials allows them to be manipulated into complex geometries; however the study of percolation in these geometries has been limited. For instance, the technique of electrospinning allows fabrication of ultrahigh aspect ratio fibers with 100 nm diameter and up to many centimeters length, which can be collected into random mats with $\geq 70\%$ porosity (Fig. 1).[7] Many society-impacting emergent applications for nanocomposite materials require such complex geometries, which may enhance or hinder the percolation process compared to a homogeneous sample. As one example, our group is interested in developing electrically conducting nanocomposite tissue scaffolds for *in vitro* electrical stimulation as a means of functional tissue engineering of bone,[8] a technique which could ultimately provide alternative bone sources for some of the 500 000 bone grafts in the U.S. per year.[9] These materials require high porosity and fiber sizes on the order of 100 nm, similar to the properties of an electrospun mat, in order to match the natural extracellular matrix which guides cells to develop or heal tissues *in vivo*. Understanding the role of this complicated microstructure, where fiber size approaches the dimensions of the particle and up to 90% void space is present, in altering or enhancing formation of conducting networks is important in developing this and other high-impact applications. Such a complex, but experimentally accessible, system offers an opportunity to further understand the fundamental process of percolation, which underlies such diverse physical phenomena as disease transmission,[10] mechanical enhancement of materials,[3] and the spread of forest fires,[11] within a constrained geometry.

We have undertaken experimental and Monte Carlo simulation studies of percolation in highly porous fibrous mats to determine the important parameters that control the critical volume fraction ρ_c, defined as the doping level where, on average, the first conducting path traversing the sample is formed. We report a direct comparison between experimental and computational studies (Fig. 2) and find good agreement. Homogeneous samples with zero, one, or two dimensions similar in size to the particle were studied by Monte Carlo simulations, along with porous samples where porosity was tuned by altering the number of fibers within the sample (holding fiber width constant) or, alternatively, adjusting the fiber width with constant fiber number. This systematic study sheds light on the interplay between the various elements of sample morphology in determining ρ_c, which is useful in comparing experimentally observed values from different constrained systems. In addition, computational studies represent an ideal case (e.g., with homogeneous fiber diameter and ideal fiber-fiber contacts) which provides information on fundamental limits, with an eye to developing composite materials where the desired properties are achieved with minimal doping.

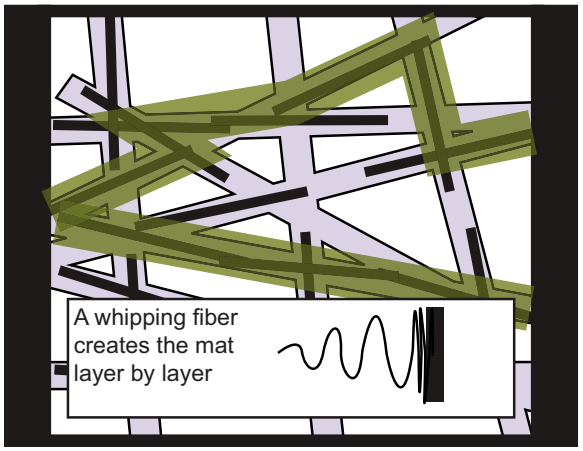

FIG. 1. (Color online) Illustration of a random mat of electrospun nanofibers doped with a large aspect ratio particle (MWNT) viewed from above. The highlighted regions depict two alternative ways to form a continuous path of particle traversing the sample, i.e., paths primarily contained within one fiber or those consisting of small regions of many fibers. The inset is a side-view illustration of the electrospun fibers being collected.

II. EXPERIMENTAL AND COMPUTATIONAL METHODS

A detailed description of sample fabrication, electrical conductivity measurements, and experimental determination of the critical volume fraction has been reported previously.[6,7,12] For Monte Carlo simulations, tests for percolation were conducted on randomly generated samples under a set of constraints (dopant size, porosity, etc.) utilizing a continuum (off-lattice) approach. For continuous films, the center point of each spherical particle was assigned using a random number generator. Overlap of up to one quarter of the particle diameter was permitted. Varying the allowed overlap from 1/16 particle diameter to no restriction did not alter the critical volume fraction for a test case. For the fibrous mats, spherical particles were randomly placed within a "fiber" slightly longer than a sample dimension. The fiber was then assigned a randomly allocated center position and orientation angle. This process models the actual experimental fabrication of the mat where a jet of particle-doped polymer solution is subjected to electrostatic forces which result in a rapid whipping action that forms an ultrathin nanocomposite fiber. Particles within the fiber which fell outside the limits of the sample after fiber placement were removed. Porosity was tuned by altering the number of fibers or, alternatively, fiber diameter. This approach reflects the tunable experimental parameters in electrospinning, where fiber diameter can be altered by adjusted spinning conditions (solution viscosity, electric-field strength, and feed rate), and fiber density is a function of deposition time and the spatial extent of the whipping region. Calculations are two dimensions except for three-dimensional (3D) continuous films. The detection of percolation (defined by at least one continuous path of particles spanning the sample space) utilized a "tree-burning" algorithm.[13] For each sample configuration, 100–1000 random configurations were generated, resulting in a graph of percolation probability versus particle loading. The

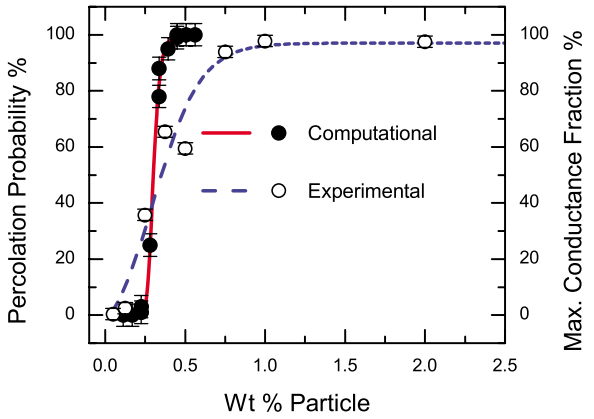

FIG. 2. (Color online) Experimental and computational results for a nanofiber mat. Computational (percolation probability %, solid circles) and experimental (maximum conductance fraction %, open circles) data are plotted against particle weight %, respectively.

critical particle number N_c was determined from the loading level with a percolation probability of 50% (Ref. 13) and normalized to account for the effect of dopant overlapping with the form $\rho_c = 1 - e^{(-\eta_c)}$, where ρ_c is the critical volume fraction.[14] η_c is the critical reduced number density, defined as $\eta_c = vN_c/V$, where V is the volume (or area) available for doping and v is the volume (area) of one particle. For porous samples, doping area was calculated from the fiber number and width, assuming a fiber length equal to the sample, and either zero or $(N/2)^2$ square fiber-fiber overlaps per fiber as an estimate of maximum and minimum areas.

To compare computational results to experimental data (which employed MWNTs), simulations of porous mats and single fibers with high aspect ratio particles were undertaken. The procedure for sample generation was unchanged from the spherical particle case aside from the addition of an orientation angle associated with the particle. In order to constrain the particle within the fibers (thus matching experimental conditions), particle placement was restricted to the center 50% of the fiber width and the orientation angle was limited such that all portions of the particle remained within the fiber. The two-dimensional (2D) computational value for the critical area fraction was extrapolated to three dimensions, assuming a sample one fiber in thickness. A maximum possible error for this extrapolation was generated by comparing with the result from continuous samples when transitioning from two dimensions to three dimensions.

III. RESULTS

A. Experimental and compuational comparison

Previously, we experimentally studied percolation within poly(ethylene oxide) fibrous mats with 75% porosity and an average fiber size of 200 ± 50 nm doped with MWNTs (average diameter of 15 nm; length of 10 μm) and determined a critical volume fraction of $(0.41 \pm 0.01)\%$ (0.45 wt % particle:polymer) or 0.10% (particle:sample space). Monte Carlo results from an equivalent system appear in Fig. 2, which yielded an estimated maximum volume of 0.30 vol %

(0.33 wt %) for one-fiber-thick samples and a lower limit of 0.10 vol %. These simulation results are in good agreement with the experimental value, which is about 30% larger than this idealized theoretical result. In the computational model, fiber-fiber contacts are ideal; however a greater level of doping may be required in the real system in order to navigate around high resistance junctions. The overall agreement of the experimental and computational results may reflect the fact that electrospun samples are fabricated by collecting a whipping fiber onto a flat plate, generating layer upon layer of random nanofibers oriented primarily within the plane of the plate with very few fibers oriented perpendicular to this plane. Thus the physical samples may be effectively quasi-two-dimensional. We note that the shape of the two curves in Fig. 2 is not expected to match. The computational data reflect the presence or absence of a single conducting path, whereas conductivity depends on the details of the particle network (i.e., the number of paths and branches) and will only plateau when the conducting pathways penetrate the majority of the sample volume.

B. Role of confinement

In order to understand the role of various constraints in determining the resultant ρ_c of a porous mat, we investigated samples with varying size and porosity to develop a qualitative and quantitative picture of the percolation process in this complex geometry. Here, spherical particles were utilized for three reasons. First, spherical dopant has only one characteristic length scale and thus can be straightforwardly compared in size to the fiber diameter. Thus this case is easily generalized, whereas ρ_c will depend on both dimensions (and the resulting aspect ratio) of a rod-shaped particle. Second, continuum results for spherical particles in one-dimensional (1D), 2D, and 3D geometries are well known and can be utilized as a check for simulation veracity. Finally, it is well known that critical volume fraction decreases rapidly with increasing particle aspect ratio.[11,13] As the introduction of porosity is generally expected to decrease ρ_c due to volume exclusion (e.g., as reported for polymer blends[15,16]), the relatively large ρ_c for spherical particles may provide a greater opportunity to observe changes due to geometrical effects.

The effect of sample size on critical volume fraction is shown in Fig. 3. Samples were constrained in zero, one, or two dimensions leaving at least one dimension much larger than that of the particle size, akin to a fiber. For a sample with a width equal to the particle diameter and a length of 20 particles, we obtain ρ_c=98% which is consistent with ρ_c =100% (Ref. 11) for a true 1D sample. As the constraint on the width is relaxed, ρ_c smoothly transitions to a value of 68% (Fig. 3), matching the known 2D continuum values which are in the range of 70%.[11] Similarly, holding the width and length at 50 particles and increasing the height further reduces the critical volume fraction toward a 3D value (data not shown). From an experimental perspective, these results indicate that fiber dimensions greater than ten times the particle size do not affect ρ_c. For sample sizes less than three times the particle diameter, the percolation process is constrained to a lower dimensionality, significantly inflating ρ_c.

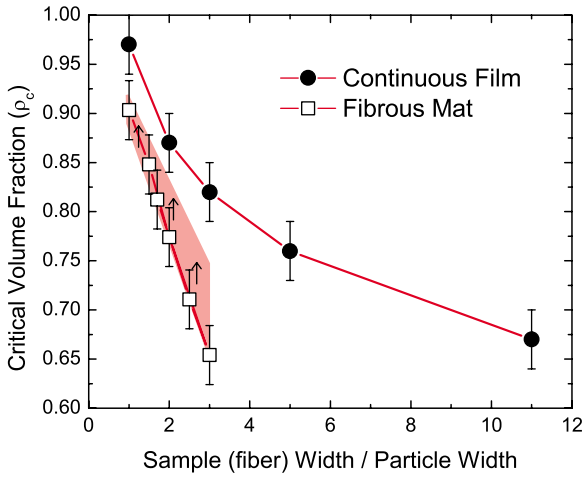

FIG. 3. (Color online) Computational data showing the change in critical volume fraction as a function of the ratio of fiber size to particle diameter. For the continuous films (single fibers), the length of the sample is held at 20 (50 in three dimensions) particle diameters while the width is varied from 1 to 11. For the porous mats, ρ_c^* is plotted versus the fiber width. The shaded area represents the range of ρ_c^* values possible from the raw data, depending on the number of fiber-fiber contacts in a particular realization. The point is for $(N/2)^2$ fiber-fiber contacts. The arrow indicates how the point shifts as the number of fiber-fiber contacts decreases.

These results can be quantified by fitting the data to a form $D=d-e^{(-x/2.96)}$, where the effective dimensionality D is a function of x, which is the ratio of the constrained sample dimension to particle diameter, and d, which is the maximum possible dimensionality (two or three) of the system. A previous study of relative sample size by Yi and Sastry[13] in a 2D square sample geometry resulted in little change in ρ_c, which is confirmed by calculations with our code (not shown). The difference between the two systems indicates that sample aspect ratio, as well as relative size, is important.

C. Role of porosity

The effect on ρ_c (dopant volume:total sample volume) due to porosity is summarized in Fig. 4(a). To aid in interpretation, we have also plotted the critical volume fraction within the polymer regions, ρ_c^* (dopant volume:polymer volume) [Fig. 4(b)]. The quantity ρ_c determines the total amount of particles needed to fabricate a conducting sample. For electrospinning fabrication, the value ρ_c^* determines the solution concentration from which fibers should be spun. In altering porosity, we began with a 70% porosity sample with a fiber size equal the particle diameter (resulting in about 15 fibers per sample) and then systematically increased the number of fibers. As an alternative, we again began with a 70% porosity sample but then increased the fiber width (keeping the fiber number constant) to decrease the porosity.

Introduction of porosity can alter the percolation process from that of a continuous film in two primary ways. First, nonzero porosity introduces void regions which cannot be doped with particle. Thus the total volume the particle network must span is reduced, which will lower ρ_c provided that

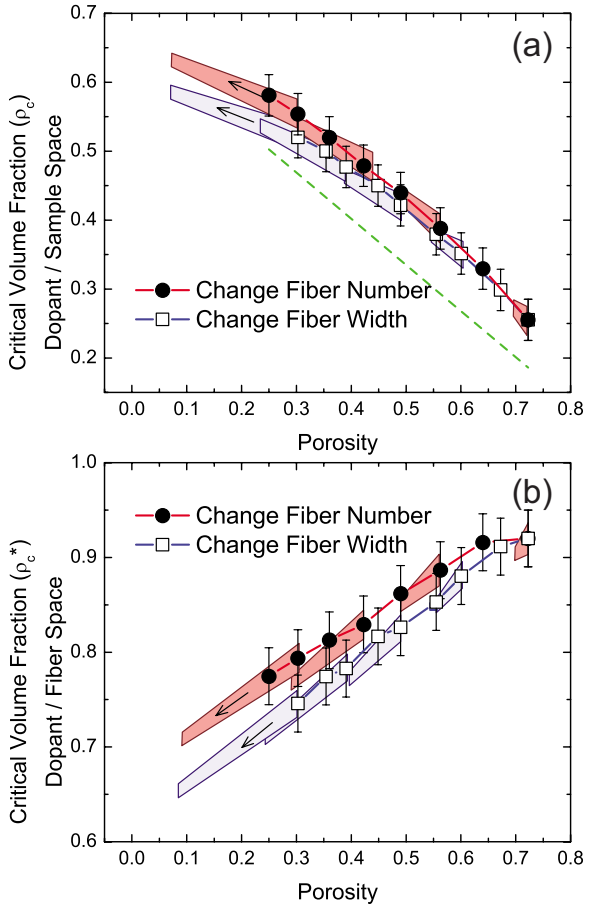

FIG. 4. (Color online) Critical volume fractions for the two series of porosity tests. The open squares represent the case of holding fiber number constant, while the filled circles are for constant fiber size. The data are represented in two ways: (a) as ρ_c (critical dopant volume/total sample volume) and (b) ρ_c^* (critical dopant volume/fiber volume). The shaded area represents the range of ρ_c (ρ_c^*) values possible from the raw data, depending on the number of fiber-fiber contacts in a particular realization. The point is for $(N/2)^2$ fiber-fiber contacts. The arrow indicates how the point shifts as the number of fiber-fiber contacts decreases. In (a), the dashed line represents the effect of volume exclusion alone.

the remaining volume (in our case, the fibers) effectively traverses the sample space. For instance, percolation will not occur even at the highest doping level if the doped regions form isolated islands. Such volume exclusion effects have been reported for three-component systems of two immiscible polymers and a particle where the particle is restricted to one polymer phase or to the interface between polymers.[15,16] As a second effect, the effective dimensionality of the sample may be reduced by this constrained volume, which will increase ρ_c^*, as seen from the studies on continuous samples (single fibers) above. Thus along with volume exclusion, which will lower ρ_c, volume confinement, a necessity if the remaining volume is to span the sample space, will tend to increase ρ_c. In summary, $\rho_c=(1-p)\rho_c^*$, where the first term accounts for volume exclusion (p is porosity) and the appropriate dimensional confinement effects are contained in ρ_c^*, with the caveat that the constrained volume must effectively span the sample space.

IV. DISCUSSION

We now apply these general observations to our particular nanocomposite system. Electrospun fibers are very long and should easily cover any reasonable sample size (<1 cm). Furthermore, the vast majority of particle is contained within the fibers. These experimental parameters have been incorporated in our computational model. Figure 4(a) summarizes ρ_c values as a function of porosity. Comparing these results to the straight line which accounts for the effect of reduction in volume, assuming no change in system dimensionality as a result, good agreement is observed. In particular, at low porosities, ρ_c scales with the inverse of doping volume. Thus, from an experimental perspective, void space can be introduced to effectively lower the amount of particle needed to establish a conducting composite. Our approach does not test composite conductivity; hence we note that such reduction in ρ_c could in principle be accompanied by a lower maximum conductivity.

In Fig. 4(a), ρ_c is elevated above the volume exclusion prediction, indicating that volume confinement effects are significant. These effects can be quantified by examining ρ_c^* [Fig. 4(b)], which reflects the process of network formation within the volume remaining for doping. We begin by discussing the possible mechanisms of path formation within a fibrous mat. At high fiber number, a percolating network within the mat can form either from small segments of many fibers or primarily within a single fiber which spans the sample (see Fig. 1). If the first process is dominant, conducting pathways can be formed in a doping regime where each fiber is still below its critical volume fraction, and thus the ρ_c^* of the mat is lower than that of a single fiber. In contrast, for the second process, these values should be similar.

Comparing ρ_c^* from the constant fiber number experiment in Fig. 4(a) and calculations for single fibers with the same sample width-particle diameter values (Fig. 3), we observe that mat values are systematically lower, indicating that multifiber pathways are significant for mats with this fiber density. This computational result is supported by our previous experimental work[6] as discussed in more detail below. Thus, decreasing fiber width constrains the doping region, reducing its effective dimensionality, in a similar manner to that of a single fiber; however, this effect is mediated by the transport mechanism within the mat, namely, percolation paths, which sample many fibers.

The mechanism for the ρ_c^* increase upon decreasing fiber number is also related to multifiber paths. As fiber number decreases, the number of possible multifiber pathways will be reduced and single fiber paths will ultimately dominate, which reduces the doping region from a quasi-two-dimensional meander to a straight line within a single fiber. In this case, $\rho_{c\,\mathrm{mat}}^*=\rho_{c\,\mathrm{fiber}}$. At very low fiber density, simulations showed that in some randomly generated configurations no fiber was oriented appropriately to provide a path traversing the sample, which was reflected in a percolation probability versus doping curve which saturated at less than 100% (data not shown). Taking the dimensionality argument further, in this case, for a single, *misoriented* fiber, the fiber is no more effective than an island in providing a sample-spanning path, and thus the mat has a dimension lower than one and an unphysical ρ_c^* of >100%.

From an experimental perspective, these results indicate that mats can percolate at lower doping levels than their component fibers. At these levels, the fibrous mat is acting as a highly porous film with an efficiently arranged dopant volume. Reduction in fiber width will decrease the effective dimensionality of the fibers, which has the effect of raising ρ_c, but the resultant volume decrease has a larger effect, and ρ_c for a porous mat will be less than that of a continuous film of the same size. Adding porosity by reducing fiber number is also effective; however, as fiber number decreases, meandering paths that utilize short sections of many fibers are limited, forcing percolation to take place through the individual fibers. At high porosities, fiber density was insufficient to provide a pathway traversing the sample.

V. CONCLUDING REMARKS

These results help us to explain the critical volume fraction observed in our experimental system. A simulation of a single fiber, with particle (MWNT) and fiber size matched to that in the experiment, yields $\rho_c=(5.8\pm0.5)\%$, significantly higher than the computational or experimental results ($\rho_c^*=0.30\%$ or 0.41%, respectively) for a random mat of such fibers. On the other hand, these mat values are greater than the expected $\rho_c=(0.1-0.2)\%$ for a three-dimensional sample doped with particles of this aspect ratio (as calculated from Celzard *et al.*[17]). 2D simulations of a continuous film, a 70% porosity fibrous mat of the same size, and a single fiber exhibit this same trend with the mat ($\rho_c^*=3.7\pm0.3$ area %) value falling between that of the film (0.7 ± 0.3 area %) and a single fiber ($54\%\pm2\%$). These basic trends, specifically, confinement effects within the fiber which raise its percolation threshold along with mat network formation that utilizes many segments of different fibers, are the same as seen in our simulations of spherical particles but complicated by the anisotropy of the MWNT. The high ρ_c value for individual fibers indicates that percolation of these long aspect ratio particles within the fibers is significantly constrained despite a nanotube diameter (15 nm) that is more than ten times less than the fiber diameter (200 nm). In contrast, the nanotube length (10 μm) is about 20 times larger than the fiber diameter, forcing significant particle alignment within each fiber. Although alignment effects have previously been studied in square (or cubic) samples,[5] in our case, alignment occurs within a long aspect ratio sample (the fiber); furthermore, averaging over the entire mat, the particles remain homogeneously distributed due to the random distribution of the fibers. The details of this confinement, including the effects of nanotube alignment, and the laminar nature of the mat samples are the subject of further work requiring extension of these simulations to fibrous systems in three dimensions, larger sample sizes, and systematic variation in particle aspect ratio.

ACKNOWLEDGMENTS

We acknowledge helpful discussions with Russell E. Gorga and use of the Beowolf cluster maintained by the College of Physical and Mathematical Sciences at NCSU.

*Corresponding author; liclarke@ncsu.edu

[1] R. Andrews and M. C. Weisenberger, Curr. Opin. Solid State Mater. Sci. **8**, 31 (2004).
[2] F. Hussain, M. Hojjati, M. Okamoto, and R. E. Gorga, J. Compos. Mater. **40**, 1511 (2006).
[3] K. I. Winey and R. A. Vaia, MRS Bull. **32**, 314 (2007).
[4] M. K. Tiwari, A. L. Yarin, and C. M. Megaridis, J. Appl. Phys. **103**, 044305 (2008).
[5] F. M. Du, J. E. Fischer, and K. I. Winey, Phys. Rev. B **72**, 121404(R) (2005).
[6] S. S. Ojha, D. R. Stevens, K. Stano, T. Hoffman, L. I. Clarke, and R. E. Gorga, Macromolecules **41**, 2509 (2008).
[7] S. D. McCullen, D. R. Stevens, W. A. Roberts, S. S. Ojha, L. I. Clarke, and R. E. Gorga, Macromolecules **40**, 997 (2007).
[8] S. D. McCullen, D. R. Stevens, W. A. Roberts, L. I. Clarke, S. H. Bernacki, R. E. Gorga, and E. G. Loboa, Nanomedicine **2**, 253 (2007).
[9] A. S. Greenwald, S. D. Boden, V. M. Goldberg, Y. Khan, C. T. Laurencin, and R. N. Rosier, J. Bone Jt. Surg., Am. Vol. **83A**, 98 (2001).
[10] C. Moore and M. E. J. Newman, Phys. Rev. E **61**, 5678 (2000).
[11] D. Stauffer and A. Aharony, *Introduction to Percolation Theory* (CRC, Philadelphia, 1994).
[12] S. D. McCullen, K. L. Stano, D. R. Stevens, W. A. Roberts, N. A. Monteiro-Riviere, L. I. Clarke, and R. E. Gorga, J. Appl. Polym. Sci. **105**, 1668 (2007).
[13] Y. B. Yi and A. M. Sastry, Phys. Rev. E **66**, 066130 (2002).
[14] J. Quintanilla, S. Torquato, and R. M. Ziff, J. Phys. A **33**, L399 (2000).
[15] P. Banerjee and B. M. Mandal, Macromolecules **28**, 3940 (1995).
[16] M. Sumita, K. Sakata, S. Asai, K. Miyasaka, and H. Nakagawa, Polym. Bull. (Berlin) **25**, 265 (1991).
[17] A. Celzard, E. McRae, C. Deleuze, M. Dufort, G. Furdin, and J. F. March, Phys. Rev. B **53**, 6209 (1996).